PERGAMON

Computers and Structures 79 (2001) 469–482

Computers & Structures

www.elsevier.com/locate/compstruc

Green's functions and boundary element method formulation for 3D anisotropic media

Fulvio Tonon [a], Ernian Pan [b,*,1], Bernard Amadei [a]

[a] Department of Civil Engineering, University of Colorado at Boulder, Boulder, CO 80309, USA
[b] Department of Mechanical Engineering, University of Colorado at Boulder, Boulder, CO 80309, USA

Received 28 December 1998; accepted 15 April 2000

Abstract

The implementation of Wang's theoretical solution is presented for elastostatic displacement Green's function for three-dimensional solids of general anisotropy. Excerpts from the authors' FORTRAN code are included. A numerical algorithm for the calculation of the derivatives of the Green's displacements and stresses is also introduced. These implementations have been incorporated into a boundary element method (BEM) code developed by the authors. The numerical results of Green's displacements, stresses and stress derivatives are in perfect agreement with closed-form solutions for transversely isotropic solids. The BEM code results are also in very close agreement with both exact solutions and other BEM formulations, even if coarse mesh discretizations are used.

Keywords: Green's displacements; Green's stresses; Green's stress derivatives; Elastic anisotropy; Boundary element method; Stress analysis

1. Introduction

Elastostatic displacement Green's functions are important in the formulation of boundary integral equations and in the solution of those equations by the boundary element method (BEM). Green's functions for 3D anisotropic media (and their simplifications under cubic and hexagonal symmetries) were apparently first derived in a seminal paper by Lifschitz and Rosenzweig in 1947 [1]. From a computational point of view, however, various numerical algorithms have been put forward [2,3] that are, in general, inefficient because of the computational burden involved.

After reviewing thoroughly this topic, Wang [4] derived explicit expressions for three-dimensional elastostatic Green's displacement in general anisotropic solids and integrals of Green's displacement derivatives over segments and rectangles. However, the Green's displacements obtained by Wang [4] are purely theoretical; no numerical implementation has been carried out so far.

At the outset, this paper reviews some of the basic concepts inherent in Wang's formulation for Green's displacements. A particularized account of the authors' implementation of these expressions follows, along with examples of the authors' own code written in FORTRAN.

A numerical algorithm for the calculation of the derivatives of the Green's displacements and stresses is subsequently introduced; it allows the discretization of the boundary to be of the most general type in a BEM formulation. The algorithm has been found to be very simple, accurate, and robust.

Finally, numerical examples of Green's displacements, stresses and stress derivatives are presented for a

* Corresponding author. Tel.: +1-919-816-0434; fax: +1-919-816-0438.

E-mail address: pan@ipass.net (E. Pan).

[1] Present address. Structures Technology, Inc., 543 Keisler Drive, Suite 204, Cary, NC 27511, USA.

0045-7949/01/$ - see front matter
PII: S0045-7949(00)00163-2

transversely isotropic solid, so as to allow a comparison with a previously available closed-form solution [5]. Numerical examples of BEM calculations are also given and the results are compared with exact solutions and previously published numerical results.

2. Outline of the analytic solution

2.1. Notation

Consider the geometry of Fig. 1a where (O, x_1, x_2, x_3) is a Cartesian coordinate system in a three-dimensional Euclidean space R^3, $(\mathbf{u}_1, \mathbf{u}_2, \mathbf{u}_3)$ is the corresponding right-handed orthonormal basis and $\mathbf{x} = (x_1, x_2, x_3)$ is a point in this space. We assume that the anisotropic body is embedded in this space.

Let $\mathbf{n} = (n_1, n_2, n_3)$ be a vector whose components in R^3 are n_1, n_2, n_3, with respect to $\mathbf{u}_1$, $\mathbf{u}_2$, $\mathbf{u}_3$, respectively. We can imagine $\mathbf{n} = (n_1, n_2, n_3)$ also as a point in a Cartesian coordinate system of a three-dimensional Euclidean space, which will be called the **n** space. Let Ω be any closed surface containing the origin of the **n** space and $d\Omega(\mathbf{n})$ an infinitesimal area element of this surface around point $\mathbf{n} = (n_1, n_2, n_3)$ as shown in Fig. 1b.

Throughout this paper, "·" indicates the dot product of two vectors and "×" indicates the cross product. Also, a comma indicates partial differentiation with respect to a variable, i.e. $f_{,i} = \partial f / \partial x_i$ and summation over repeated indices is assumed.

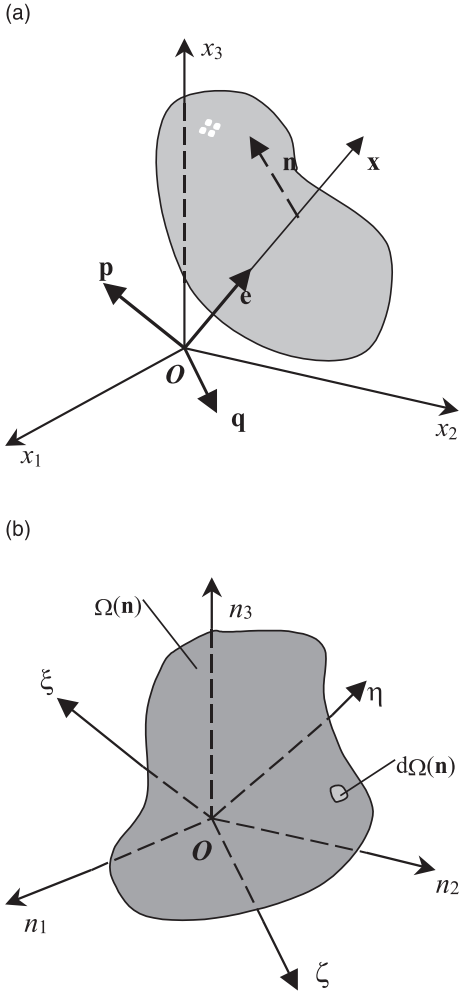

Fig. 1. (a) Anisotropic elastic body (shown bounded for representation convenience) referred to a fixed Cartesian system. Vectors **p**, **q**, and **e** are defined in Appendix B. (b) Closed surface Ω containing the origin in the **n** space.

2.2. Basic equations

Consider an unbounded homogeneous anisotropic linearly elastic solid subjected to a point load in the fixed coordinate system (O, x_1, x_2, x_3) of Fig. 1a. Green's function will be denoted by $g_{pk}(\mathbf{x})$ and gives the displacement in the x_p direction at **x** produced by a point load applied at the origin O in the x_k direction. Let σ_{ij} be the stress tensor, u_i the displacement field and

$$\varepsilon_{pq} = 0.5\left(u_{p,q} + u_{q,p}\right) \tag{1a}$$

the infinitesimal strain. The stresses and strains are related as follows:

$$\sigma_{ij} = c_{ijpq}\varepsilon_{pq}, \tag{1b}$$

where c_{ijpq} is the elastic tensor, which is fully symmetric and positive definite.

Inserting the kinematics relation (1a) into the constitutive relation (1b) and the latter into the equilibrium equation, one obtains the following three second-order partial differential equations (F_i is the body force per unit volume):

$$c_{ijpq}u_{p,jq} + F_i = 0 \tag{2}$$

once the symmetry of the elastic tensor is taken into account. Because Green's function is relative to a point force, Eq. (2) becomes

$$c_{ijpq}g_{pk,jq}(\mathbf{x}) = -\delta_{ik}\delta(\mathbf{x}), \tag{3}$$

where δ_{ik} is the Kronecker delta and $\delta(\mathbf{x})$ the Dirac delta function.

In the subsequent implementation, the 6×6 matrix **D** of elastic constants is introduced such that

$$\sigma_k = \mathbf{D}\varepsilon_k, \tag{4}$$

where $\sigma_k = (\sigma_{11k}, \sigma_{22k}, \sigma_{33k}, \sigma_{23k}, \sigma_{13k}, \sigma_{12k})^{\mathrm{T}}$ is Green's stress vector (relative to a point force applied

in direction k at the origin) and $\varepsilon_k = (\varepsilon_{11k}, \quad \varepsilon_{22k}, \quad \varepsilon_{33k}, \quad 2\varepsilon_{23k}, \quad 2\varepsilon_{13k}, \quad 2\varepsilon_{12k})^{\mathrm{T}}$ is Green's strain vector (relative to a point force applied in direction k at the origin) with its components being defined as

$$\varepsilon_{ijk} = 0.5\big(g_{ik,j} + g_{jk,i}\big). \tag{5}$$

The components c_{ijks} are related to the elastic constants $D_{\alpha\beta}$ by means of well-known relationships [6].

2.3. Analytic solution

We notice that $c_{ijpq}n_jn_q$ is symmetric and positive definite, so that its inverse is well defined. We set

$$\Gamma_{ip}(\mathbf{n}) = c_{ijpq}n_jn_q, \qquad \Gamma^{-1}_{ip}(\mathbf{n}) = \big(c_{ijpq}n_jn_q\big)^{-1}. \tag{6}$$

Consider now the following identities, in which integration is taken in the $\mathbf{n}$ space over any closed surface Ω including the origin (Fig. 1b) and use is made of Eqs. (A.6b) and (A.8) (see Appendix A):

$$\begin{aligned} c_{irps}\frac{\partial^2}{\partial x_r\,\partial x_s}\int_\Omega \Gamma^{-1}_{pk}(\mathbf{n})\delta(\mathbf{n}\cdot\mathbf{x})\,\mathrm{d}\Omega(\mathbf{n}) &= c_{irps}\int_\Omega \Gamma^{-1}_{pk}(\mathbf{n})n_rn_s\frac{\mathrm{d}^2\delta(s)}{\mathrm{d}s^2}\bigg|_{s=\mathbf{n}\cdot\mathbf{x}}\mathrm{d}\Omega(\mathbf{n}) \\ &= \int_\Omega c_{irps}n_rn_s\big(c_{prqs}n_rn_s\big)^{-1}\frac{\mathrm{d}^2\delta(s)}{\mathrm{d}s^2}\bigg|_{s=\mathbf{n}\cdot\mathbf{x}}\mathrm{d}\Omega(\mathbf{n}) \\ &= \delta_{ik}\int_\Omega \frac{\mathrm{d}^2\delta(s)}{\mathrm{d}s^2}\bigg|_{s=\mathbf{n}\cdot\mathbf{x}}\mathrm{d}\Omega(\mathbf{n}) \\ &= \delta_{ik}\nabla\int_\Omega \frac{\delta(\mathbf{n}\cdot\mathbf{x})}{|\mathbf{n}|^2}\,\mathrm{d}\Omega(\mathbf{n}). \end{aligned} \tag{7}$$

Since the last member in Eq. (7) can be written in terms of the plane representation of the delta function (A.10), we have

$$c_{irps}\frac{\partial^2}{\partial x_r\,\partial x_s}\int_\Omega \Gamma^{-1}_{pk}(\mathbf{n})\delta(\mathbf{n}\cdot\mathbf{x})\,\mathrm{d}\Omega(\mathbf{n}) = -8\pi^2\delta_{ik}\delta(\mathbf{x}). \tag{8}$$

Comparing Eq. (3) with Eq. (8), we get the following integral expression for Green's displacement function:

$$g_{pk}(\mathbf{x}) = \frac{1}{8\pi^2}\int_\Omega \Gamma^{-1}_{pk}(\mathbf{n})\delta(\mathbf{n}\cdot\mathbf{x})\,\mathrm{d}\Omega(\mathbf{n}). \tag{9}$$

We now try to write Eq. (9) in a form suitable for integration by means of the residue theorem. To this end, we express the inverse tensor $\Gamma^{-1}_{pk}(\mathbf{n})$ as

$$\Gamma^{-1}_{pk}(\mathbf{n}) = \frac{A_{pk}(\mathbf{n})}{D(\mathbf{n})}, \tag{10}$$

where $A_{pk}(\mathbf{n})$ and $D(\mathbf{n})$ are the adjoint matrix and the determinant of $c_{ijpq}n_jn_q$, respectively.

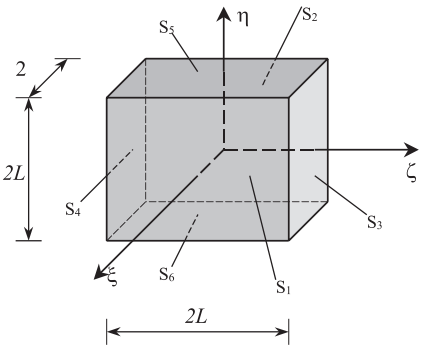

Fig. 2. Parallelepiped over which contour integration is taken in the $\mathbf{n}$ space. The surfaces S_1 and S_2 are bounded by $\xi = \pm 1$, S_3 and S_4 by $\zeta = \pm L$, S_5 and S_6 by $\eta = \pm L$.

It is convenient to use the coordinates (ξ, ζ, η) introduced in Appendix B. Using Eq. (B.4), Eq. (9) becomes

$$g_{pk}(\mathbf{x}) = \frac{1}{8\pi^2}\int_\Omega \frac{A_{pk}(\xi\mathbf{p}+\zeta\mathbf{q}+\eta\mathbf{e})}{D(\xi\mathbf{p}+\zeta\mathbf{q}+\eta\mathbf{e})}\delta(r\eta)\,\mathrm{d}\Omega(\xi,\zeta,\eta), \tag{11}$$

where r is the distance between the field and source points (see Eq. (B.1a)).

Since $\Gamma_{pk}(\mathbf{n})$ is a 3×3 matrix, each entry of its adjoint matrix A_{pk} is a polynomial of order 4 in ξ, ζ and η. Similarly, determinant $D(\mathbf{n})$ is a polynomial of order 6 in ξ, ζ and η.

Following Wang [4], we choose Ω as a rectangular parallelepiped having size $2L\times 2L\times 2$ (Fig. 2) and let the dimension L go to infinity. Since over surfaces other than S_1 and S_2 the integrand in Eq. (11) approaches zero as $1/L^2$, the contribution of the integration over every surface but S_1 and S_2 vanishes. Moreover, the integrand in Eq. (11) is symmetric with respect to ξ, since only even powers of ξ are involved. This leads to twice the integration over $S_1(\xi = 1)$:

$$\begin{aligned} g_{pk}(\mathbf{x}) &= \frac{1}{4\pi^2}\int_{S_1}\frac{A_{pk}(\mathbf{p}+\zeta\mathbf{q}+\eta\mathbf{e})}{D(\mathbf{p}+\zeta\mathbf{q}+\eta\mathbf{e})}\delta(r\eta)\mathrm{d}\Omega(\xi,\zeta,\eta) \\ &= \frac{1}{4\pi^2}\int_{-\infty}^{\infty}\int_{-\infty}^{\infty}\frac{A_{pk}(\mathbf{p}+\zeta\mathbf{q}+\eta\mathbf{e})}{D(\mathbf{p}+\zeta\mathbf{q}+\eta\mathbf{e})}\delta(r\eta)\mathrm{d}\zeta\,\mathrm{d}\eta \\ &= \frac{1}{4\pi^2 r}\int_{-\infty}^{\infty}\frac{A_{pk}(\mathbf{p}+\zeta\mathbf{q})}{D(\mathbf{p}+\zeta\mathbf{q})}\,\mathrm{d}\zeta. \end{aligned} \tag{12}$$

The integral in Eq. (12) can be handled by means of the residue theorem. The poles are the roots of the polynomial equation of sixth order in ζ:

$$D(\mathbf{p}+\zeta\mathbf{q}) = 0. \tag{13}$$

If $\mathbf{n}\neq\mathbf{0}$ is real, $\Gamma_{pk}(\mathbf{n})$ is a real symmetric, positive definite matrix; thus, its determinant can never be zero

for $\mathbf{n} \neq \mathbf{0}$. For Eq. (13) to be satisfied, ζ must therefore be complex. A corollary of the fundamental theorem of algebra [7] tells us that a real polynomial of order N has N roots and that if $\zeta = a + \mathrm{i}b$ is a root, its conjugate $\zeta^* = a - \mathrm{i}b$ must also be a root [7]. In the present case, there are three roots ζ_m satisfying,

$$D(\mathbf{p} + \zeta_m \mathbf{q}) = 0 \tag{14}$$

with

$$\operatorname{Im} \zeta_m > 0, \quad m = 1, 2, 3 \tag{15}$$

and we may write

$$D(\mathbf{p} + \zeta \mathbf{q}) = \sum_{k=0}^{6} a_{k+1} \zeta^k = a_7 \prod_{m=1}^{3} (\zeta - \zeta_m)(\zeta - \zeta_m^*), \tag{16}$$

where a_k are the coefficients of the sextic polynomial $D(\mathbf{p} + \zeta \mathbf{q})$ with respect to ζ. Eq. (13) is called the sextic equation of elasticity and it has been shown that no closed-form solution exists for its roots for general anisotropy [8]. Thus, this equation must be solved numerically. Integral (12) can now be expressed in terms of the residues at the poles, taking into account that it must be real:

$$g_{pk}(\mathbf{x}) = -\frac{\operatorname{Im}}{2\pi r} \sum_{m=1}^{3} \frac{A_{pk}(\mathbf{p} + \zeta_m \mathbf{q})}{a_7 (\zeta_m - \zeta_m^*) \prod_{\substack{k=1 \\ k \neq m}}^{3} (\zeta_m - \zeta_k)(\zeta_m - \zeta_k^*)}. \tag{17}$$

In deriving Green's displacement (17), we have assumed that all the roots of the sextic equation are distinct. Should the roots be multiple, a slight change in the elastic constants will result in single roots, with negligible errors in the computed Green's tensor.

Some features of formula (17) need to be pointed out:

1. since $\Gamma_{pk}(\mathbf{n})$ is symmetric, its adjoint matrix A_{pk} is also symmetric and so is the Green's tensor g_{pk}. As a consequence, only six terms out of nine must be calculated;
2. for two points $\mathbf{x}_1$ and $\mathbf{x}_2$ aligned along the same line passing through the origin, the summation over index m has the same value;
3. as a consequence of (2), g_{pk} approaches zero as $1/r$ when $r \to \infty$;
4. as a consequence of (2), g_{pk} depends only on the relative position of the source point and field point. Thus, the implementation can proceed considering the source point always at the origin, by an applicable translation; this leads to an important simplification of the implementation itself;
5. the numerical solution of a polynomial of sixth order is the only numerical step required in order to obtain the entire Green's function.

3. Implementation of the analytic solution

The key steps in the implementation of the analytic formulation fall essentially into two groups:

1. entries of $\Gamma_{ij}(\mathbf{p} + \zeta \mathbf{q})$ in terms of elastic constants $D_{\alpha\beta}$, coordinates of field point $\mathbf{x}$, and variable ζ;
2. coefficients a_i ($i = 1$–7) of the sextic polynomial (16).

In order to keep the expressions as simple as possible, vector $\mathbf{v}$ introduced in Appendix B must coincide with one of the base vectors $\mathbf{u}_1$, $\mathbf{u}_2$, and $\mathbf{u}_3$. In the following, we have assumed that $\mathbf{v}$ is either (1, 0, 0) or (0, 1, 0); the choice between them must be made on the basis of $\mathbf{x}$ and affects step 1 only.

3.1. Entries of matrix $\Gamma_{ij}(\boldsymbol{p} + \zeta \boldsymbol{q})$

Each entry of matrix $\Gamma_{ij}(\mathbf{p} + \zeta \mathbf{q})$ is a polynomial of order two in ζ of the form:

$$\Gamma_{ij}(\mathbf{p} + \zeta \mathbf{q}) = b_{ij1} + b_{ij2}\zeta + b_{ij3}\zeta^2. \tag{18}$$

As an example, coefficients b_{1jk} are given in Appendix C in FORTRAN format for the case when $\mathbf{v} = (1, 0, 0)$; they are functions of the entries of matrix $\mathbf{D}$, which are much more manageable than the fourth-order tensor c_{ijpq}. Coefficients b_{ijk} are also functions of the field point coordinates. The correspondence between notation used in the text and notation used in the FORTRAN code is established in Table 1. MATHEMATICA 2.2 was used to get the expression of coefficients b_{ijk}.

3.2. Coefficients of the sextic polynomial

Although it is possible to get the expressions of coefficients a_i ($i = 1$–7) directly in terms of the elastic constants $D_{\alpha\beta}$ and of the field point coordinates, this leads to expressions as long as 40 pages, which cannot be handled easily by the compiler and are not computationally efficient. Thus, the idea is to derive them in terms of the b_{ijk} coefficients introduced in Eq. (18). Determinant $D(\mathbf{p} + \zeta \mathbf{q})$ can in fact be written as the sum of trinomials:

Table 1
Correspondence between notation used in the text and notation used in the FORTRAN code

Notation used in the text	Notation used in the FORTRAN code
b_{ijk}	`b(i,j,k)`
D_{ij}	`cd(i,j)`
$x = (x_1, x_2, x_3)$	`xf,yf,zf`
a_i	`a(i)`

$$D(\mathbf{p}+\zeta\mathbf{q}) = -\Gamma_{13}\Gamma_{22}\Gamma_{31} + 2\Gamma_{12}\Gamma_{23}\Gamma_{31} - \Gamma_{11}\Gamma_{23}\Gamma_{32} - \Gamma_{12}\Gamma_{21}\Gamma_{33} + \Gamma_{11}\Gamma_{22}\Gamma_{33}. \tag{19}$$

If we put Eq. (18) into Eq. (19), we realize that each coefficient a_i (relative to ζ^{i-1}) is a sum of trinomials of b_{ijk} coefficients. Let l, m, n be the last indexes of the coefficients of a trinomial, we found that these indexes have to satisfy $l+m+n=i-2$ in order for the product to be of order $i-1$. For example, only coefficients b_{ijk} such that $k=1$ contribute to a_1. Thus, in general,

$$a_i = -\sum_{l,m,n:l+m+n=i-2} b_{13i}b_{22j}b_{31k} + 2\sum_{l,m,n:l+m+n=i-2} b_{12i}b_{23j}b_{31k} - \sum_{l,m,n:l+m+n=i-2} b_{11i}b_{23j}b_{32k} - \sum_{l,m,n:l+m+n=i-2} b_{12i}b_{21j}b_{33k} + \sum_{l,m,n:l+m+n=i-2} b_{11i}b_{22j}b_{33k}. \tag{20}$$

Examples of coefficients a_i ($i=1$–4) calculated according to Eq. (20) are given in Appendix D in FORTRAN format (see Table 1 for notation correspondence). It is to be noted that the present implementation of the analytic solution is quite simple, when compared to the complexity of the problem in hand.

4. Derivatives of the Green's displacements and stresses

Analytic solutions for the integral over segments and rectangles of the Green's displacement derivatives were proposed by Wang [4]. However, expressions of the derivatives of the Green's displacements are necessary if the boundary discretization must be more general. Several attempts were made by the authors in order to get a closed-form solution of the Green's function derivatives. The most promising of them started from the derivation of Eq. (12) and led to the expression:

$$g_{pk,s}(\mathbf{x}) = \frac{x_s}{2\pi r^3}\operatorname{Im}\sum_{m=1}^{3}\frac{A_{pk}(\mathbf{p}+\zeta_m\mathbf{q})}{a_7(\zeta_m-\zeta_m^*)\prod_{\substack{k=1\\k\neq m}}^{3}(\zeta_m-\zeta_k)(\zeta_m-\zeta_k^*)} - \frac{1}{2\pi r}\operatorname{Im}\sum_{m=1}^{3}\frac{\frac{\partial A_{pk}(\mathbf{p}+\zeta_m\mathbf{q})}{\partial x_s}}{a_7(\zeta_m-\zeta_m^*)\prod_{\substack{k=1\\k\neq m}}^{3}(\zeta_m-\zeta_k)(\zeta_m-\zeta_k^*)} + \frac{1}{2\pi r}\operatorname{Im}\sum_{m=1}^{3}\lim_{\zeta\to\zeta_m}\frac{\mathrm{d}}{\mathrm{d}\zeta}\left[(\zeta-\zeta_m)^2\frac{A_{pk}}{D^2}\frac{\partial D}{\partial x_s}\right]. \tag{21}$$

In this equation, the last term is very complicated, therefore, a numerical algorithm based on the Lagrange polynomials was proposed [9]. Despite of its simplicity, this approach has been proven to be efficient, accurate, and robust [9].

Following [9], let a function $f(x)$ be known at n points $x_1 < x_2 < \cdots < x_n$. Let us call $y_i = f(x_i)$ $i=1,\ldots,n$ and set

$$F(x) = \prod_{k=1}^{n}(x-x_k); \qquad F_k(x) = \prod_{\substack{r=1\\r\neq k}}^{n}(x-x_r);$$

$$F_k(x_k) = \prod_{\substack{r=1\\r\neq k}}^{n}(x_k-x_r). \tag{22}$$

The complete Lagrange interpolation function is

$$f(x) = P(x) + F(x)\cdot\frac{f^{(n)}(\xi(x))}{n!}, \tag{23}$$

where

$$P(x) = \sum_{k=1}^{n}\frac{F_k(x)}{F_k(x_k)}\cdot y_k. \tag{24}$$

By taking the derivative of Eq. (23) and evaluating it at x_r, we get

$$f'(x_r) = P'(x_r) + F'(x_r)\cdot\frac{f^{(n)}(\xi(x_r))}{n!}. \tag{25}$$

Thus, the error in the first derivative is

$$F'(x_r)\cdot\frac{f^{(n)}(\xi(x_r))}{n!}, \tag{26}$$

where $F'(x_r)$ is nothing but the product of the distances between x_r and the other chosen abscissas. Therefore, if the intervals between the chosen abscissas is constant, its minimum value is attained at the mid point (or two mid-points if n is even) of the segment between x_1 and x_n. It follows that the best approximation of the value of $f'(x_r)$ obtainable using the polynomial derivative is attained at the mid-point (or two mid-points if n is even) of the segment between x_1 and x_n. It can be shown that the derivative of the Lagrange polynomial is

$$P'(x_r) = \sum_{\substack{k=1\\k\neq r}}^{n}\frac{1}{x_r-x_k}\left[y_r - y_k\frac{F'(x_r)}{F'(x_k)}\right]. \tag{27}$$

If we choose a polynomial of order 2, i.e. 3 abscissas, from Eqs. (25) and (27), we get

$$f'(x_2) = \frac{1}{2h}[-f(x_1)+f(x_3)] - \frac{h^2}{6}f^{(3)}(\xi_2), \tag{28}$$

where h is the distance between two consecutive abscissas and ξ_2 is a point comprised between x_1 and x_3.

Now, let $\mathbf{x}$ be the field point at which we want to calculate Green's stress component σ_{ijk} defined in Section 2.2. To this end, the expression of Green's strain component ε_{ijk} at $\mathbf{x}$ is necessary in order to calculate σ_{ijk} by means of Eq. (4). Using Eq. (28), the following

expressions of Green's strain component ε_{ijk} at $\mathbf{x}$ are obtained:

$$\varepsilon_{11k}(\mathbf{x}) \approx \frac{g_{1k}(\mathbf{x}+\Delta_1) - g_{1k}(\mathbf{x}-\Delta_1)}{2h}, \tag{29}$$

$$\varepsilon_{22k}(\mathbf{x}) \approx \frac{g_{2k}(\mathbf{x}+\Delta_2) - g_{2k}(\mathbf{x}-\Delta_2)}{2h}, \tag{30}$$

$$\varepsilon_{33k}(\mathbf{x}) \approx \frac{g_{3k}(\mathbf{x}+\Delta_3) - g_{3k}(\mathbf{x}-\Delta_3)}{2h}, \tag{31}$$

$$\varepsilon_{23k}(\mathbf{x}) \approx \frac{g_{3k}(\mathbf{x}+\Delta_2) - g_{3k}(\mathbf{x}-\Delta_2) + g_{2k}(\mathbf{x}+\Delta_3) - g_{2k}(\mathbf{x}-\Delta_3)}{4h}, \tag{32}$$

$$\varepsilon_{13k}(\mathbf{x}) \approx \frac{g_{1k}(\mathbf{x}+\Delta_3) - g_{1k}(\mathbf{x}-\Delta_3) + g_{3k}(\mathbf{x}+\Delta_1) - g_{3k}(\mathbf{x}-\Delta_1)}{4h}, \tag{33}$$

$$\varepsilon_{12k}(\mathbf{x}) \approx \frac{g_{1k}(\mathbf{x}+\Delta_2) - g_{1k}(\mathbf{x}-\Delta_2) + g_{2k}(\mathbf{x}+\Delta_1) - g_{2k}(\mathbf{x}-\Delta_1)}{4h}, \tag{34}$$

where $\Delta_1 = (h,0,0)$, $\Delta_2 = (0,h,0)$, $\Delta_3 = (0,0,h)$.

In order to get the complete Green's stress and strain at point $\mathbf{x}$, it is thus necessary to compute the Green's tensor at six points in the neighborhood of $\mathbf{x}$. The choice of interval h is a crucial decision. An extensive numerical investigation has led us to the conclusion that the best value of the interval is

$$h = r \times 10^{-6}, \tag{35}$$

where r is the distance between the field and source points.

It is also noteworthy that the attempts aimed at increasing the accuracy of the approximation by adding other terms to Eqs. (29)–(34) led to no appreciable improvement. In the authors' opinion, the reason for the good performance of this scheme lies primarily in the smooth and monotonic behavior of Green's displacements.

In order to calculate the internal stresses, the derivatives of Green's stresses and displacements are needed with respect to the coordinates of the source point (see Section 5). By virtue of observation 4 in Section 2, these derivatives are equal but opposite in sign to the derivatives taken with respect to the field point x_i. According to Eq. (28), the derivatives of Green's stresses are approximated as

$$\sigma_{ijk,l}(\mathbf{x}) \approx \frac{\sigma_{ijk}(\mathbf{x}+\Delta_l) - \sigma_{ijk}(\mathbf{x}-\Delta_l)}{2h}, \quad l = 1,2,3, \tag{36a}$$

and the derivatives of Green's displacements as

$$g_{ij,l}(\mathbf{x}) \approx \frac{g_{ij}(\mathbf{x}+\Delta_l) - g_{ij}(\mathbf{x}-\Delta_l)}{2h}, \quad l = 1,2,3. \tag{36b}$$

5. Boundary element method formulation

Consider an elastic body (finite or infinite) with the following displacement and traction conditions imposed on the boundary $\Gamma = \Gamma_u + \Gamma_t$:

$$u_j(\mathbf{x}) = \overline{u}_j(\mathbf{x}), \quad \mathbf{x} \in \Gamma_u, \tag{37a}$$

$$\sigma_{ij}(\mathbf{x}) n_j(\mathbf{x}) = \overline{T}_j(\mathbf{x}), \quad \mathbf{x} \in \Gamma_t \tag{37b}$$

with n_j being the external normal to Γ_t.

For each internal point $\mathbf{x}_p$ the following integral equation holds [10]:

$$u_i(\mathbf{x}_p) + \int_\Gamma T^*_{ij}(\mathbf{x}_p,\mathbf{x}) u_j(\mathbf{x})\,\mathrm{d}\Gamma(\mathbf{x}) = \int_\Gamma U^*_{ij}(\mathbf{x}_p,\mathbf{x}) T_j(\mathbf{x})\,\mathrm{d}\Gamma(\mathbf{x}), \tag{38}$$

where $U^*_{ij}(\mathbf{x}_p,\mathbf{x})$ and $T^*_{ij}(\mathbf{x}_p,\mathbf{x})$ are Green's displacements and tractions, respectively. By virtue of observation 4 in Section 2, $U^*_{ij}(\mathbf{x}_p,\mathbf{x})$ and $T^*_{ij}(\mathbf{x}_p,\mathbf{x})$ are equal to

$$U^*_{ij}(\mathbf{x}_p,\mathbf{x}) = g_{ij}(\mathbf{x}-\mathbf{x}_p), \tag{39}$$

$$T^*_{ij}(\mathbf{x}_p,\mathbf{x}) = \sigma_{ikj}(\mathbf{x}-\mathbf{x}_p) n_k(\mathbf{x}). \tag{40}$$

If $\mathbf{x}_p$ approaches a point $\mathbf{x}_\mathrm{b}$ on the boundary, Eq. (38) must be replaced by

$$d_{ij} u_j(\mathbf{x}_\mathrm{b}) + \int_\Gamma T^*_{ij}(\mathbf{x}_\mathrm{b},\mathbf{x}) u_j(\mathbf{x})\,\mathrm{d}\Gamma(\mathbf{x}) = \int_\Gamma U^*_{ij}(\mathbf{x}_\mathrm{b},\mathbf{x}) T_j(\mathbf{x})\,\mathrm{d}\Gamma(\mathbf{x}), \tag{41}$$

where d_{ij} are coefficients that depend only on the local geometry of the boundary at $\mathbf{x}_\mathrm{b}$.

The term on the right-hand side of Eq. (41) has weak singularity (see observation 3, Section 2) and can thus be integrated by means of a usual Gauss quadrature technique. The rigid-body motion method [10,11] can be used to overcome the Cauchy-type singularity in the first integrand and at the same time to avoid the calculation of coefficients d_{ij}.

Eq. (41) can be discretized and, once boundary conditions (37) are taken into account, the resulting algebraic system of equations can be solved for the un-

known boundary displacements and tractions. Then, Eq. (38) can be used to calculate the internal displacements.

In order to get the internal stresses, it is necessary to take the derivative of Eq. (38) with respect to the internal coordinates $\mathbf{x}_p$. This yields [11]

$$u_{i,l}(\mathbf{x}_p) + \int_\Gamma T^*_{ij,l}(\mathbf{x}_p,\mathbf{x})u_j(\mathbf{x})\,\mathrm{d}\Gamma(\mathbf{x}) = \int_\Gamma U^*_{ij,l}(\mathbf{x}_p,\mathbf{x})T_j(\mathbf{x})\,\mathrm{d}\Gamma(\mathbf{x}), \tag{42}$$

where

$$T^*_{ij,l}(\mathbf{x}_p,\mathbf{x}) = -\sigma_{ikj,l}(\mathbf{x}-\mathbf{x}_p)n_k(\mathbf{x}), \tag{43a}$$

$$U^*_{ij,l}(\mathbf{x}_p,\mathbf{x}) = -g_{ij,l}(\mathbf{x}-\mathbf{x}_p) \tag{43b}$$

with $\sigma_{ikj,l}(\mathbf{x}-\mathbf{x}_p)$ given by Eq. (36a) and $g_{ij,l}(\mathbf{x}-\mathbf{x}_p)$ by Eq. (36b).

Once $u_{i,l}(\mathbf{x}_p)$ are obtained, the internal stresses are calculated by means of the following equation similar to Eqs. (4) and (5):

$$\sigma = \mathbf{D}\varepsilon, \tag{44a}$$

where

$$\sigma = (\sigma_{11},\quad \sigma_{22},\quad \sigma_{33},\quad \sigma_{23},\quad \sigma_{13},\quad \sigma_{12})^{\mathrm{T}}, \tag{44b}$$

$$\varepsilon = (\varepsilon_{11},\quad \varepsilon_{22},\quad \varepsilon_{33},\quad 2\varepsilon_{23},\quad 2\varepsilon_{13},\quad 2\varepsilon_{12})^{\mathrm{T}}, \tag{44c}$$

$$\varepsilon_{ij} = \tfrac{1}{2}(u_{i,j}+u_{j,i}). \tag{44d}$$

The implementation described in Sections 3 and 4 was incorporated into an existing three-dimensional BEM code (see Ref. [11] for its description) according to the procedure presented in this Section. In Ref. [11], only transversely isotropic 3D media (with any oriented plane of transverse isotropy) was considered and implemented in the code; in this paper, Wang's solution for generally anisotropic media has been implemented.

6. Numerical examples

6.1. Green's displacements, stresses and derivatives of the stresses

Let us consider a transversely isotropic and linearly elastic solid, whose plane of transverse isotropy is parallel to the x_1x_2 plane. A closed-form solution exists in this case for the Green's displacements, stresses [5] and derivatives of the stresses [11]. This solution will be used (as implemented in Ref. [11]) to validate the proposed formulation.

The material properties are as follows: $E = 20\times 10^4$ kN/m^2, $E' = 4\times 10^4$ kN/m^2, $\nu = 0.25$, $\nu' = 0.25$, $G' = 1.6\times 10^4$ kN/m^2, where E and E' are Young's moduli in the plane of transverse isotropy and in the direction normal to it, respectively; ν and ν' are the Poisson's ratios characterizing the lateral strain response in the plane of transverse isotropy to a stress acting parallel and normal to it, respectively; and G' is the shear modulus in planes normal to the plane of symmetry. The corresponding elastic-constant matrix $\mathbf{D}$ is (only the upper half is given)

$$\begin{pmatrix} 88 & 72 & 40 & 0 & 0 & 0 \\ & 88 & 40 & 0 & 0 & 0 \\ & & 24 & 0 & 0 & 0 \\ & & & 16 & 0 & 0 \\ & \text{sym.} & & & 16 & 0 \\ & & & & & 8 \end{pmatrix} \times 10^4 \text{ kN/m}^2. \tag{45}$$

The field point is placed at $\mathbf{x} = (-1, 0.8, 1.5)$ m. The displacements, stresses, stress derivatives are listed in Tables 2–4, respectively. The agreement between the closed-form solution and the present formulation is very good for all three quantities. Only for some components of the derivatives of the stresses (Table 4) is the relative difference not negligible; however, it must be noted that the magnitude of these components is small with respect to the remaining components, thus leading to negligible

Table 2
Green's displacements ($\times 10^{-4}$ m) calculated according to Pan's and Chou's closed-form solution [5] as implemented in Ref. [11] and with the present formulation. The source point is at the origin, the field point is at $\mathbf{x} = (-1, 0.8, 1.5)$ m

(i, j)	g_{ij} transversely isotropic formulation	g_{ij} present formulation	Relative difference
1, 1	4.0141588565E−03	4.0141588610E−03	1.1E−09
1, 2	−2.9315529284E−04	−2.9315529143E−04	4.8E−09
1, 3	−2.1517885087E−03	−2.1517885172E−03	3.9E−09
2, 1	−2.9315529284E−04	−2.9315529143E−04	4.8E−09
2, 2	3.8822389747E−03	3.8822389799E−03	1.3E−09
2, 3	1.7214308070E−03	1.7214308137E−03	3.9E−09
3, 1	−2.1517885087E−03	−2.1517885172E−03	3.9E−09
3, 2	1.7214308070E−03	1.7214308137E−03	3.9E−09
3, 3	1.9003220124E−02	1.9003220284E−02	8.4E−09

Table 3
Green's stresses (kN/m^2) calculated according to Pan's and Chou's closed-form solution [5] as implemented in Ref. [11] and the present formulation. The source point is at the origin, the field point in $\mathbf{x} = (-1, 0.8, 1.5)$ m

ijk	σ_{ijk} transversely isotropic formulation	σ_{ijk} present formulation	Relative difference
111	3.0534645334E−03	3.0534575287E−03	2.3E−06
221	5.5516532436E−03	5.5516460542E−03	1.3E−06
331	6.9594542712E−03	6.9594505349E−03	5.4E−07
231	2.5160305656E−03	2.5160307422E−03	7.0E−08
131	−3.3933330101E−03	−3.3933332396E−03	6.8E−08
121	−1.8033628216E−03	−1.8033626725E−03	8.3E−08
112	−5.6717491681E−03	−5.6717487868E−03	6.7E−08
222	−1.2123450534E−03	−1.2123450967E−03	3.6E−08
332	−5.5675634169E−03	−5.5675634915E−03	1.3E−08
232	−2.2611192556E−03	−2.2611192104E−03	2.0E−08
132	2.5160305656E−03	2.5160306251E−03	2.4E−08
122	7.1617031049E−04	7.1617003567E−04	3.8E−07
113	−1.7147827999E−02	−1.7147807646E−02	1.2E−06
223	−8.3655438558E−03	−8.3655210747E−03	2.7E−06
333	−2.2078536037E−02	−2.2078524002E−02	5.4E−07
233	−1.1775219220E−02	−1.1775219467E−02	2.1E−08
133	1.4719024025E−02	1.4719024871E−02	5.7E−08
123	1.9516186984E−02	1.9516189072E−02	1.1E−07

Table 4
Derivatives of the Green's stresses (kN/m^3) calculated according to the exact closed-form solution derived and implemented in Ref. [11] and the present formulation. The source point is at the origin, the field point in $\mathbf{x} = (-1, 0.8, 1.5)$ m

ijk, *l*	$\sigma_{ijk,l}$ transversely isotropic formulation	$\sigma_{ijk,l}$ present formulation	Relative difference
111, 1	−0.59622259271E−02	−0.59629572705E−02	1.2E−04
111, 2	−0.45086940696E−02	−0.45074656599E−02	−2.7E−04
111, 3	−0.56414664921E−02	−0.56411267186E−02	−6.0E−05
221, 1	0.44694421882E−02	0.44685063303E−02	−2.0E−04
221, 2	−0.11811731607E−02	−0.11798500052E−02	−1.1E−03
221, 3	−0.37926171802E−02	−0.37921063932E−02	−1.3E−04
331, 1	0.16987884233E−02	0.16982433466E−02	−3.2E−04
331, 2	−0.69265941556E−02	−0.69258768984E−02	−1.0E−04
331, 3	−0.44525631963E−02	−0.44523121121E−02	−5.6E−05
231, 1	0.79385810234E−03	0.79379727638E−03	−7.7E−05
231, 2	0.49712727263E−03	0.49714271358E−03	3.1E−05
231, 3	−0.30906032310E−02	−0.30906216080E−02	5.9E−06
131, 1	0.39554359236E−02	0.39554842055E−02	1.2E−05
131, 2	0.18677123922E−02	0.18676962357E−02	−8.6E−06
131, 3	0.61652880201E−02	0.61653303015E−02	6.8E−06
121, 1	0.42717763920E−02	0.42718112393E−02	8.1E−06
121, 2	−0.20306209291E−03	−0.20300240322E−03	−2.9E−04
121, 3	0.53606344730E−02	0.53607252836E−02	1.7E−05
112, 1	−0.30768883497E−02	−0.30775369921E−02	2.1E−04
112, 2	0.84038676742E−03	0.84094663232E−03	6.7E−04
112, 3	0.50628670483E−02	0.50629208004E−02	1.6E−05
222, 1	−0.26129788805E−02	−0.26137365442E−02	2.9E−04
222, 2	−0.48936107600E−02	−0.48931499059E−02	−9.4E−05
222, 3	0.24843998895E−02	0.24845314971E−02	5.3E−05
332, 1	−0.69265941556E−02	−0.69269468094E−02	5.9E−05
332, 2	−0.14181789466E−02	−0.14179740950E−02	−1.4E−04
332, 3	0.35620505570E−02	0.35621376993E−02	2.4E−05

Table 4 (*continued*)

ijk, *l*	$\sigma_{ijk,l}$ transversely isotropic formulation	$\sigma_{ijk,l}$ present formulation	Relative difference
232, 1	−0.84519058971E−03	−0.84518000388E−03	−1.2E−05
232, 2	−0.43559086593E−02	−0.43559177742E−02	2.9E−06
232, 3	0.47745165660E−02	0.47746037165E−02	1.8E−05
132, 1	0.79385810234E−03	0.79378559587E−03	−9.1E−05
132, 2	0.49712727263E−03	0.49718754586E−03	1.2E−04
132, 3	−0.30906032312E−02	−0.30906169537E−02	4.4E−06
122, 1	0.11909419404E−03	0.11905631360E−03	−3.2E−04
122, 2	0.61674915810E−02	0.61674862040E−02	−8.7E−07
122, 3	−0.41648264611E−02	−0.41648490465E−02	5.4E−06
113, 1	0.71134008460E−02	0.71131995957E−02	−2.8E−05
113, 2	0.33341653291E−01	0.33342792915E−01	3.4E−05
113, 3	0.98238228068E−02	0.98259170804E−02	2.1E−04
223, 1	−0.29318534460E−01	−0.29319149219E−01	3.0E−05
223, 2	−0.15577546399E−01	−0.15576273564E−01	−8.2E−05
223, 3	−0.83606419668E−04	−0.81186914690E−04	−2.9E−02
333, 1	−0.27302017639E−01	−0.27302079852E−01	2.3E−06
333, 2	0.21841614111E−01	0.21842236628E−01	2.8E−05
333, 3	−0.41215790310E−03	−0.41093285237E−03	−3.0E−03
233, 1	−0.14561076074E−01	−0.14560962479E−01	−7.8E−06
233, 2	−0.30701631651E−02	−0.30703156075E−02	5.0E−05
233, 3	0.76303285982E−02	0.76304202029E−02	1.2E−05
133, 1	0.34823210683E−02	0.34819436621E−02	−1.1E−04
133, 2	−0.14561076074E−01	−0.14560935326E−01	−9.7E−06
131, 3	−0.95379107477E−02	−0.95379106793E−02	−7.2E−09
123, 1	0.79472178014E−02	0.79465584372E−02	−8.3E−05
123, 2	0.24245099017E−02	0.24250012946E−02	2.3E−04
123, 3	−0.22016509392E−01	−0.22016463462E−01	−2.1E−06

errors in the computation of the internal stresses, as will be shown in Section 6.2.

6.2. Boundary element method models

The following two examples have the same geometry. A cube of transversely isotropic material, whose edge is 1 m long, is discretized very coarsely with six nine-node isoparametric elements and with a total of 26 nodes (Fig. 3). The faces of the block are parallel to the coordinate planes. The block is subjected to a uniform compression of 1 kN/m^2 on the two faces parallel to the x_1x_2 plane. For this case, an exact solution exists [12].

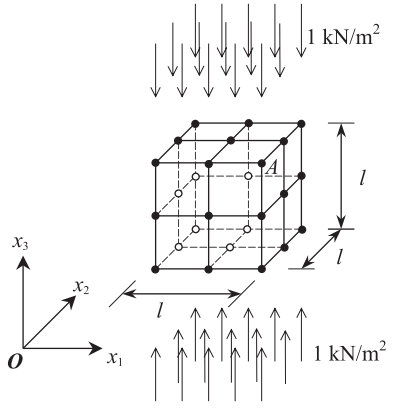

Fig. 3. Cube having edge of length $l = 1$ m discretized with six nine-node quadrilateral elements with a total of 26 nodes.

In the first example, we adopt the same material constants as considered in Section 6.1. However, the plane of symmetry is no longer parallel to the x_1x_2 plane, but is inclined with a dip direction angle $\varphi = 60^\circ$ and a dip angle $\psi = 45^\circ$ (Fig. 4). Consequently, the elastic-constant matrix **D** referred to the x_1, x_2, and x_3 axes is now fully populated (only the upper half is given):

$$\begin{pmatrix} 14.5 & 9.9 & 9.6 & -0.2 & -3.1177 & -1.5588 \\ & 18.5 & 9.6 & -2.2 & -1.0392 & -1.9052 \\ & & 12.8 & -1.6 & -2.7713 & 0 \\ & & & 3.2 & 0 & -1.0392 \\ & \text{sym.} & & & 3.2 & -0.2 \\ & & & & & 3.5 \end{pmatrix} \times 10^4 \text{ kN/m}^2. \tag{46}$$

This case was also considered in [11] where it was solved using the closed-form Green's displacements, stresses [5]

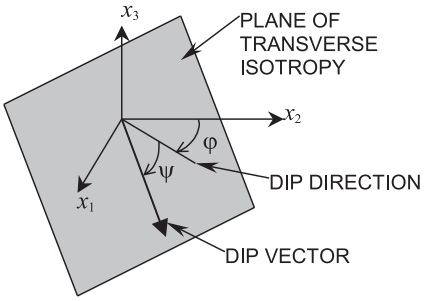

Fig. 4. Orientation of the plane of transverse isotropy. Dip angle ψ is the angle between the plane of symmetry and x_1x_2 plane; dip direction angle φ is the angle between x_2 and the orthogonal projection of the dip vector on the x_1x_2 plane. Positive angles are shown.

and stress derivatives [11]. The results obtained with these formulations and with the present one are listed in Tables 5 and 6; they indicate that for both the displacements (on the boundary and internal) and internal stresses, the exact values, the values calculated with the present implementation and the values calculated in Ref. [11] are in very good agreement.

The second example resembles the one reported in Ref. [13]. Here, a (transversely isotropic) zinc cube is considered, whose plane of symmetry is parallel to the x_1x_2 plane. The elastic-constant matrix referred to the x_1, x_2, and x_3 axes is now (only the upper half is given)

$$\begin{pmatrix} 161.00 & 34.20 & 50.10 & 0 & 0 & 0 \\ & 161.00 & 50.10 & 0 & 0 & 0 \\ & & 61.00 & 0 & 0 & 0 \\ & & & 38.3 & 0 & 0 \\ & & & & 38.30 & 0 \\ & & & & & 63.40 \end{pmatrix} \text{GPa}. \tag{47}$$

It is to be noted that zinc has a negative Poisson ratio $\nu_{12} = -0.06$. In Table 7, the results obtained by Schclar [13] with a different numerical formulation for general anisotropic bodies are given in the second column. Comparison between columns 1 and 3 and 2 and 3 indicates that the present formulation and implementation is much more precise.

Table 5
Block under uniform compression. Example 1: surface displacements at node A ($\times 10^{-5}$ m)

	Present	Transversely isotropic formulation [11]	Exact [12]
u_1	−0.5496	−0.5496	−0.5496
u_2	−0.7029	−0.7032	−0.7031
u_3	−1.0417	−1.0417	−1.0417

Table 6
Block under uniform compression. Example 1: internal displacements along the vertical center line (Panel A) and stresses along the vertical centerline (Panel B–D)

z (m)	Present	Transversely isotropic formulation [11]	Exact [12]
Panel A: u_3 ($\times 10^{-5}$ m)			
0.75	−0.5210	−0.5208	−0.5209
0.625	−0.2604	−0.2604	−0.2604
0.5	0.0000	0.0000	0.0000
0.375	0.2604	0.2604	0.2604
0.25	0.5208	0.5208	0.5208
Panel B: σ_{11} (kN/m^2)			
0.75	0.0005	0.0011	0.0000
0.625	0.0006	−0.0000	0.0000
0.5	−0.0023	−0.0000	0.0000
0.375	0.0096	−0.0000	0.0000
0.25	0.0013	0.0014	0.0000
Panel C: σ_{22} (kN/m^2)			
0.75	−0.0060	−0.0040	0.0000
0.625	−0.0021	−0.0000	0.0000
0.5	−0.0007	0.0000	0.0000
0.375	0.0084	−0.0000	0.0000
0.25	−0.0045	−0.0044	0.0000
Panel D: σ_{33} (kN/m^2)			
0.75	−0.999	−1.001	−1.000
0.625	−0.992	−1.000	−1.000
0.5	−1.002	−1.000	−1.000
0.375	−1.000	−1.000	−1.000
0.25	−1.003	0.988	−1.000

Table 7
Zinc block under uniform compression. Example 2: boundary displacements at node A ($\times 10^{-7}$ m)

	Present	Anisotropic formulation [13]	Exact [12]
u_1	7.278	7.291	7.274
u_2	−7.277	−7.291	−7.274
u_3	−28.35	−28.42	−28.34

7. Conclusions

The implementation of a theoretical solution for Green's displacements in general anisotropic solids is presented. Its detailed illustration has been accompanied with excerpts from the authors' own FORTRAN code, in order for the implementation to be available and readily usable by as many readers as possible. Many features distinguish the present implementation from existing numerical formulations:

1. the procedure is completely analytic, the only numerical step is associated with the determination of the roots of a sixth-order polynomial;

2. once the roots of this polynomial are known, the entire Green's tensor is immediately calculated;
3. the procedure is very robust, since no problem arose even with transversely isotropic materials;
4. the implementation is very efficient, since less than 16 s were necessary to run 10,000 calculations of the entire Green's tensor in a PC featuring a 266 MHz Pentium II processor and 64 MB RAM;
5. an extensive numerical validation (one example of which was included in the paper) has shown its high accuracy.

A numerical algorithm has also been proposed for Green's stresses and their derivatives. Despite its simplicity, it has been proven to be

1. robust, since no problem arose even with transversely isotropic materials;
2. very accurate even with degenerate (transversely isotropic) materials and/or when the field point is very close to or very far from the source point;
3. very efficient, since less than 80 s were necessary to run 10,000 calculations of the complete Green's stresses in a PC featuring a 266 MHz Pentium II processor and 64 MB RAM.

The performance of the proposed implementations within a previously developed three-dimensional BEM code [11] turned out to be highly accurate when compared to both exact solutions and transversely isotropic BEM formulations for which closed-form expressions of Green's displacements, stresses and stress derivatives were used. When compared to previously published results obtained with completely different numerical formulations, the present implementation turned out to be much more precise.

Finally, our Green's functions have just been successfully implemented into a general program called BEFE, a coupled boundary and finite element program developed by Beer and co-workers [14]. While BEFE program will now be applied to solve more complex problems involving material anisotropy [15], a comparison study of our Green's function implementation with others [16] is currently under investigation. Also, the authors are looking at the possible advantages in implementing the recent developments in the analysis of anisotropic media using Stroh's formalism [17,18]. The explicit three-dimensional Green's function in a general anisotropic infinite space was derived by Ting and Lee [17] using the Stroh eigenvalues.

Acknowledgements

This work was supported by the National Science Foundation under Grant No. CMS-9713559 and the Air Force Office of Scientific Research under Grant F49620-98-1-0104. The authors would like to thank Dr. C.Y. Wang, currently with Schlumberger, for his stimulating discussion. The useful recommendations of the anonymous reviewers are also greatly appreciated.

Appendix A. Radon transform and plane representation of the Dirac delta function

The Radon transform [19–23] is of fundamental importance in order to work out the analytic solution of the problem at hand.

Let $f(\mathbf{x})$ be a function defined in R^3 and s a real number; the Radon transform of $f(\mathbf{x})$ is defined as

$$\hat{f}(s,\mathbf{n}) = R[f(\mathbf{x})] = \int f(\mathbf{x}) \cdot \delta(s - \mathbf{n}\cdot\mathbf{x})\,\mathrm{d}\mathbf{x}, \tag{A.1}$$

where $\delta(\ )$ is the one-dimensional Dirac delta function.

It follows that, when s varies over the real line, the Radon transform is an integration of $f(\mathbf{x})$ over all planes defined by $\mathbf{n}\cdot\mathbf{x} = s$, i.e., having normal $\mathbf{n}$ and distant $s/|\mathbf{n}|$ from the origin O.

The *inverse Radon transform* is an integration in the $\mathbf{n}$ space over the closed surface Ω containing the origin and defined as

$$f(\mathbf{x}) = R^*\left(\hat{f}''\right) = -\frac{1}{8\pi^2}\int_\Omega \hat{f}''(\mathbf{n}\cdot\mathbf{x},\mathbf{n})\,\mathrm{d}\Omega(\mathbf{n}), \tag{A.2}$$

where

$$\hat{f}''(\mathbf{n}\cdot\mathbf{x},\mathbf{n}) = \left.\frac{\partial^2 \hat{f}(s,\mathbf{n})}{\partial s^2}\right|_{s=\mathbf{n}\cdot\mathbf{x}}. \tag{A.3}$$

Let $\delta(\mathbf{x}) = \delta(x_1,x_2,x_3)$ be the Dirac delta centered in the origin, i.e. the functional

$$\int_{R^3} \delta(\mathbf{x}) f(\mathbf{x})\,\mathrm{d}V = f(\mathbf{o}), \tag{A.4}$$

where $\mathbf{o} = (0,0,0)$.

We will use the same symbol δ for both one-dimensional and three-dimensional Dirac delta, with the convention that if the argument is a scalar, the one-dimensional Dirac delta is involved and if the argument is a vector, the three-dimensional Dirac delta is involved.

The Radon transform of the Dirac delta is

$$\begin{aligned}\hat{\delta}(s,\mathbf{n}) &= R[\delta(\mathbf{x})] = \int \delta(\mathbf{x})\cdot\delta(s-\mathbf{n}\cdot\mathbf{x})\,\mathrm{d}\mathbf{x}\\ &= \delta(s-\mathbf{n}\cdot\mathbf{o}) = \delta(s).\end{aligned} \tag{A.5}$$

Now

$$\frac{\partial\delta(\mathbf{n}\cdot\mathbf{x})}{\partial x_i} = n_i \left.\frac{\mathrm{d}\delta}{\mathrm{d}s}\right|_{s=\mathbf{n}\cdot\mathbf{x}},$$
$$\frac{\partial^2\delta(\mathbf{n}\cdot\mathbf{x})}{\partial x_i^2} = n_i^2 \left.\frac{\mathrm{d}^2\delta}{\mathrm{d}^2 s}\right|_{s=\mathbf{n}\cdot\mathbf{x}}. \quad \text{(A.6a, b)}$$

Thus,

$$\sum_{i=1}^{3}\frac{\partial^2\delta(\mathbf{n}\cdot\mathbf{x})}{\partial x_i^2} = \sum_{i=1}^{3} n_i^2 \left.\frac{\mathrm{d}^2\delta}{\mathrm{d}s^2}\right|_{s=\mathbf{n}\cdot\mathbf{x}} = \left.\frac{\mathrm{d}^2\delta}{\mathrm{d}s^2}\right|_{s=\mathbf{n}\cdot\mathbf{x}} \sum_{i=1}^{3} n_i^2 = |\mathbf{n}|^2 \left.\frac{\mathrm{d}^2\delta}{\mathrm{d}s^2}\right|_{s=\mathbf{n}\cdot\mathbf{x}}. \quad \text{(A.7)}$$

Since the first member of Eq. (A.7) is Laplacian of δ, $\Delta\delta$, Eq. (A.3) becomes

$$\hat{\delta}'' = \left.\frac{\mathrm{d}^2\delta}{\mathrm{d}s^2}\right|_{s=\mathbf{n}\cdot\mathbf{x}} = \frac{\Delta\delta(\mathbf{n}\cdot\mathbf{x})}{|\mathbf{n}|^2}. \quad \text{(A.8)}$$

According to Eq. (A.2), the inverse Radon transform is

$$\delta(\mathbf{x}) = -\frac{1}{8\pi^2}\int_{\Omega}\frac{\Delta\delta(\mathbf{n}\cdot\mathbf{x})}{|\mathbf{n}|^2}\,\mathrm{d}\Omega(\mathbf{n}) = -\frac{1}{8\pi^2}\Delta\int_{\Omega}\frac{\delta(\mathbf{n}\cdot\mathbf{x})}{|\mathbf{n}|^2}\,\mathrm{d}\Omega(\mathbf{n}), \quad \text{(A.9)}$$

the last passage is due to the fact that the variable of integration is **n**, not **x**.

Thus, we have the very notable relation, called "plane representation for $\delta(\mathbf{x})$":

$$\delta(\mathbf{x}) = -\frac{1}{8\pi^2}\Delta\int_{\Omega}\frac{\delta(\mathbf{n}\cdot\mathbf{x})}{|\mathbf{n}|^2}\,\mathrm{d}\Omega(\mathbf{n}) \quad \text{(A.10)}$$

that coincides with Eq. (6) in Wang [4].

Appendix B. Change of coordinate system

The Radon transform is an integration over the planes whose normal is **n**. The inverse Radon transform, for a fixed **x**, is an integration involving all the normal vectors **n**. Therefore, a convenient coordinate system when we perform the inverse transform is such that an axis is parallel to **x** [4] (Fig. 1a). Let us define

$$r = |\mathbf{x}|, \quad \mathbf{e} = \frac{\mathbf{x}}{r}. \quad \text{(B.1)}$$

If **v** is an arbitrary unit vector different from **e** ($\mathbf{v} \neq \mathbf{e}$), two normal vectors orthogonal to **e** are

$$\mathbf{p} = \frac{\mathbf{e}\times\mathbf{v}}{|\mathbf{e}\times\mathbf{v}|}, \quad \text{(B.2)}$$

$$\mathbf{q} = \mathbf{e}\times\mathbf{p}. \quad \text{(B.3)}$$

Let ξ, ζ, η be the components of *vector* **n** in the new coordinate system of R^3, then

$$\mathbf{n} = \xi\mathbf{p} + \zeta\mathbf{q} + \eta\mathbf{e}, \quad \text{(B.4a)}$$

$$\mathbf{n}\cdot\mathbf{x} = \mathbf{p}\cdot\mathbf{x}\xi + \mathbf{q}\cdot\mathbf{x}\zeta + \mathbf{e}\cdot\mathbf{x}\eta = r\eta. \quad \text{(B.4b)}$$

This transformation induces a transformation of coordinates in the **n** space with (ξ, ζ, η) being the coordinates of *point* **n** in the new coordinate system in the **n** space as shown in Fig. 1b. The determinant of the Jacobian of the latter transformation is obviously equal to 1.

Appendix C. Coefficients $\mathbf{b}_{1jk}$

If $\mathbf{v} = (1, 0, 0)$ then

```
      b(1, 1, 1)=(yf**2*cd(5,
     5)-2*yf*zf*cd(5, 6)+zf**2*cd(6, 6))/
     (yf**2+zf**2)
c
      b(1, 1, 2)=2*(yf**3*cd(1, 5)
     +yf*zf**2*cd(1, 5)-yf**2*zf*cd(1, 6)
     -zf**3*cd(1, 6)-xf*yf*zf*cd(5, 5)
     -xf*yf**2*cd(5, 6)+xf*zf**2*cd(5, 6)
     +xf*yf*zf*cd(6, 6))/((yf**2+zf**2)
     *Sqrt(xf**2+yf**2+zf**2))
c
      b(1, 1, 3)=(yf**4*cd(1, 1)
     +2*yf**2*zf**2*cd(1, 1)+zf**4*cd(1, 1)
     -2*xf*yf**2*zf*cd(1, 5)
     -2*xf*zf**3*cd(1, 5)-2*xf*yf**3*cd(1, 6)
     -2*xf*yf*zf**2*cd(1, 6)
     +xf**2*zf**2*cd(5, 5)
     +2*xf**2*yf*zf*cd(5, 6)
     +xf**2*yf**2*cd(6, 6))/
     ((yf**2+zf**2)*(xf**2+yf**2+zf**2))
c
      b(1, 2, 1)=(-(yf*zf*cd(2, 5))
     +zf**2*cd(2, 6)+yf**2*cd(4, 5)
     -yf*zf*cd(4, 6))/(yf**2+zf**2)
c
      b(1, 2, 2)=(-(yf**2*zf*cd(1, 2))
     -zf**3*cd(1, 2)+yf**3*cd(1, 4)
     +yf*zf**2*cd(1, 4)-xf*yf**2*cd(2, 5)
     +xf*zf**2*cd(2, 5)+2*xf*yf*zf*cd(2, 6)
     -2*xf*yf*zf*cd(4, 5)- xf*yf**2*cd(4, 6)
     +xf*zf**2*cd(4, 6)+yf**3*cd(5, 6)
     +yf*zf**2*cd(5, 6)-yf**2*zf*cd(6, 6)
     -zf**3*cd(6, 6))/((yf**2+zf**2)
     *Sqrt(xf**2+yf**2+zf**2))
```

```
c
      b(1, 2, 3)=(-(xf*yf**3*cd(1, 2))
     -xf*yf*zf**2*cd(1, 2)-xf*yf**2*zf*cd(1, 4)
     -xf*zf**3*cd(1, 4)+yf**4*cd(1, 6)
     +2*yf**2*zf**2*cd(1, 6)+zf**4*cd(1, 6)
     +xf**2*yf*zf*cd(2, 5)+xf**2*yf**2*cd(2, 6)
     +xf**2*zf**2*cd(4, 5)+xf**2*yf*zf*cd(4, 6)
     -xf*yf**2*zf*cd(5, 6)- xf*zf**3*cd(5, 6)
     -xf*yf**3*cd(6, 6)-xf*yf*zf**2*cd(6, 6))/
     ((yf**2+zf**2)*(xf**2+yf**2+zf**2))
c
      b(1, 3, 1)=(yf**2*cd(3, 5)-
     yf*zf*cd(3, 6)-yf*zf*cd(4, 5)
     +zf**2*cd(4, 6))/(yf**2+zf**2)
c
      b(1, 3, 2)=(yf**3*cd(1, 3)
     +yf*zf**2*cd(1, 3)- yf**2*zf*cd(1, 4)
     -zf**3*cd(1, 4)-2*xf*yf*zf*cd(3, 5)-
     xf*yf**2*cd(3, 6)+xf*zf**2*cd(3, 6)
     -xf*yf**2*cd(4, 5)+xf*zf**2*cd(4, 5)
     +2*xf*yf*zf*cd(4, 6)+yf**3*cd(5, 5)
     +yf*zf**2*cd(5, 5)-yf**2*zf*cd(5, 6)
     -zf**3*cd(5, 6))/
     ((yf**2+zf**2)*Sqrt(xf**2+yf**2+zf**2))
c
      b(1, 3, 3)=(-(xf*yf**2*zf*cd(1, 3))-
     xf*zf**3*cd(1, 3)-xf*yf**3*cd(1, 4)
     -xf*yf*zf**2*cd(1, 4)+yf**4*cd(1, 5)
     +2*yf**2*zf**2*cd(1, 5)+zf**4*cd(1, 5)
     +xf**2*zf**2*cd(3, 5)+xf**2*yf*zf*cd(3, 6)
     +xf**2*yf*zf*cd(4, 5)+xf**2*yf**2*cd(4, 6)
     - xf*yf**2*zf*cd(5, 5)-xf*zf**3*cd(5, 5)
     -xf*yf**3*cd(5, 6)-xf*yf*zf**2*cd(5,
     6))/((yf**2+zf**2)*(xf**2+yf**2+zf**2))
```

Appendix D. Examples of coefficients a_i ($i = 1$–4)

```
      a(1)=-(b(1, 3, 1)*b(2, 2, 1)*b(3, 1, 1))
     +2*b(1, 2, 1)*b(2, 3, 1)*b(3, 1, 1)
     b(1, 1, 1)*(2, 3, 1)*b(3, 2, 1)b(1, 2, 1)
     *b(2, 1, 1)*b(3, 3, 1)+b(1, 1, 1)
     *b(2, 2, 1)*b(3, 3, 1)
c
      a(2)=-(b(1, 3, 2)*b(2, 2, 1)*b(3, 1, 1)
     +b(1, 3, 1)*b(2, 2, 2)*b(3, 1, 1)
     +b(1, 3, 1)*b(2, 2, 1)*b(3, 1, 2))
     +2*(b(1, 2, 2)*b(2, 3, 1)*b(3, 1, 1)
     +b(1, 2, 1)*b(2, 3, 2)*b(3, 1, 1)
     +b(1, 2, 1)*b(2, 3, 1)*b(3, 1, 2))(b(1, 1, 2)
     *b(2, 3, 1)*b(3, 2, 1)+b(1, 1, 1)*b(2, 3,
     2)*b(3, 2, 1)+b(1, 1, 1)*b(2, 3, 1)*b(3, 2,
     2))(b(1, 2, 2)*b(2, 1, 1)*b(3, 3, 1)
     +b(1, 2, 1)*b(2, 1, 2)*b(3, 3, 1)+b(1, 2, 1)
     *b(2, 1, 1)*b(3, 3, 2))+(b(1, 1, 2)*b(2, 2, 1)
     *b(3, 3, 1)+b(1, 1, 1)*b(2, 2, 2)*b(3, 3, 1)
     +b(1, 1, 1)* b(2, 2, 1)* b(3, 3, 2))
c
      a(3)=-(b(1, 3, 3)*b(2, 2, 1)*b(3, 1, 1)
     +b(1, 3, 1)*b(2, 2, 3)*b(3, 1, 1)
     +b(1, 3, 1)*b(2, 2, 1)*b(3, 1, 3)+b(1, 3, 2)
     *b(2, 2, 2)*b(3, 1, 1)+b(1, 3, 1)*b(2, 2, 2)
     *b(3, 1, 2)+b(1, 3, 2)*b(2, 2, 1)*b(3, 1, 2))
     +2*(b(1, 2, 3)*b(2, 3, 1)*b(3, 1, 1)
     +b(1, 2, 1)*b(2, 3, 3)*b(3, 1, 1)+b(1, 2, 1)
     *b(2, 3, 1)*b(3, 1, 3)+b(1, 2, 2)*b(2, 3, 2)
     *b(3, 1, 1)+b(1, 2, 1)*b(2, 3, 2)*b(3, 1, 2)
     +b(1, 2, 2)*b(2, 3, 1)*b(3, 1, 2))(b(1, 1, 3)
     *b(2, 3, 1)*b(3, 2, 1)+b(1, 1, 1)*b(2, 3, 3)
     *b(3, 2, 1)+b(1, 1, 1)*b(2, 3, 1)*b(3, 2, 3)
     +b(1, 1, 2)*b(2, 3, 2)*b(3, 2, 1)
     +b(1, 1, 1)*b(2, 3, 2)*b(3, 2, 2)
     +b(1, 1, 2)*b(2, 3, 1)*b(3, 2, 2))-(b(1, 2, 3)
     *b(2, 1, 1)*b(3, 3, 1)+b(1, 2, 1)b(2, 1, 3)
     b(3, 3, 1)+b(1, 2, 1)*b(2, 1, 1)*b(3, 3, 3)
     +b(1, 2, 2)*b(2, 1, 2)*b(3, 3, 1)+b (1, 2, 1)
     *b(2, 1, 2)*b(3, 3, 2)+b(1, 2, 2)*b(2, 1, 1)
     *b(3, 3, 2))+ (b(1, 1, 3)*b(2, 2, 1)*b(3, 3, 1)
     + b(1, 1, 1)*b(2, 2, 3)*b(3, 3, 1)+b(1, 1, 1)
     *b(2, 2, 1)*b(3, 3, 3)+b(1, 1, 2)*b(2, 2, 2)
     *b(3, 3, 1)+b(1, 1, 1)*b(2, 2, 2)*b(3, 3, 2)
     + b(1, 1, 2)*b(2, 2, 1)*b(3, 3, 2))
c
      a(4)=- (b(1, 3, 3)*b(2, 2, 2)*b(3, 1, 1)
     +b(1, 3, 2)*b(2, 2, 3)*b(3, 1, 1)+b(1, 3, 1)
     *b(2, 2, 2)*b(3, 1, 3)+b(1, 3, 1)*b(2, 2, 3)
     *b(3, 1, 2)+b(1, 3, 2)*b(2, 2, 1)*b(3, 1, 3)
     +b(1, 3, 3)*b(2, 2, 1)*b(3, 1, 2)
     +b(1, 3, 2)*b(2, 2, 2)*b(3, 1, 2))
     +2*(b(1, 2, 3)*b(2, 3, 2)*b(3, 1, 1)
     +b(1, 2, 2)*b(2, 3, 3)*b(3, 1, 1)+b(1, 2, 1)
     *b(2, 3, 2)*b(3, 1, 3)+b(1, 2, 1)*b(2, 3, 3)
     *b(3, 1, 2)+b(1, 2, 2)*b(2, 3, 1)*b(3, 1, 3)
     +b(1, 2, 3)*b(2, 3, 1)*b(3, 1, 2)
     +b(1, 2, 2)*b(2, 3, 2)*b(3, 1, 2))(b(1, 1, 3)
     *b(2, 3, 2)*b(3, 2, 1)+b(1, 1, 2)*b(2, 3, 3)
     *b(3, 2, 1)+b(1, 1, 1)*b(2, 3, 2)*b(3, 2, 3)
     +b(1, 1, 1)*b(2, 3, 3)*b(3, 2, 2)
     +b(1, 1, 2)*b(2, 3, 1)*b(3, 2, 3)+b(1, 1, 3)
     *b(2, 3, 1)*b(3, 2, 2)+b(1, 1, 2)*b(2, 3, 2)
     *b(3, 2, 2)(b(1, 2, 3)*b(2, 1, 2)*b(3, 3, 1)
     +b(1, 2, 2)*b(2, 1, 3)*b(3, 3, 1)
     +b(1, 2, 1)*b(2, 1, 2)*b(3, 3, 3)+b(1, 2, 1)
     *b(2, 1, 3)*b(3, 3, 2)+b(1, 2, 2)*b(2, 1, 1)
     *b(3, 3, 3)+b(1, 2, 3)*b(2, 1, 1)*b(3, 3, 2)
     +b(1, 2, 2)*b(2, 1, 2)*b(3, 3, 2))
     +(b(1, 1, 3)*b(2, 2, 2)*b(3, 3, 1)
     +b(1, 1, 2)*b(2, 2, 3)*b(3, 3, 1)
     +b(1, 1, 1)*b(2, 2, 2)*b(3, 3, 3)
     +b(1, 1, 1)*b(2, 2, 3)*b(3, 3, 2)
     +b(1, 1, 2)*b(2, 2, 1)*b(3, 3, 3)
     +b(1, 1, 3)*b(2, 2, 1)*b(3, 3, 2)
     +b(1, 1, 2)*b(2, 2, 2)*b(3, 3, 2))
```

References

[1] Lifshitz IM, Rozenzweig LN. On the construction of the Green's tensor for the basic equation of the theory of elasticity of an anisotropic infinite medium. J Exp Theor Phys JETP 1947;17:783–91.
[2] Synge JL. The hypercircle in mathematical physics. Cambridge, UK: Cambridge University Press; 1957.
[3] Mura T. Micromechanics and defects in solids. 2nd ed. Martinus Nijhoff, 1987.
[4] Wang C-Y. Elastic fields produced by a point source in solids of general anisotropy. J Eng Math 1997;32:41–52.
[5] Pan YC, Chou TW. Point force solution for an infinite transversely isotropic solid. J Appl Mech 1976;29:225–36.
[6] Ting TCT. Anisotropic elasticity – theory and applications. New York: Oxford University Press; 1996.
[7] Barozzi E, Gonzales E. Calculus, vol. 1. Padova: Edizioni Libreria Progetto; 1989.
[8] Head AK. The Gaois unsolvability of the sextic equation of anisotropic elasticity. J Elasticity 1979;9:9–20.
[9] Pan E, Tonon F. Three-dimensional Green's functions in anisotropic piezoelectric solids. Int J Solids Struct 2000; 37:943–58.
[10] Brebbia CA, Dominguez J. Boundary elements, an introductory course. New York: McGraw Hill; 1989.
[11] Pan E, Amadei B. 3-D boundary element formulation of anisotropic elasticity with gravity. Appl Math Model 1996;20:114–20.
[12] Lekhnitskii SG. Theory of elasticity of an anisotropic elastic body. San Francisco: Holden-Day; 1963.
[13] Schclar NA. Anisotropic analysis using boundary elements. Topics in engineering, vol. 20. Southampton, UK: Computational Mechanics Publications, 1994.
[14] Beer G. BEFE users manual, CSS, Carnerigasse 10, Graz, Austria, 1998.
[15] Tonon F, Amadei B. A numerical study on weakness detection ahead of the tunnel face. Proc Fourth North American Rock Mech. Symp Pacific Rocks: Rock Around the Rim, University of Washington, Washington, USA, 31 July–3 August 2000, Rotterdam: Balkema, in press.
[16] Sales MA, Gray LJ. Evaluation of the anisotropic Green's function and its derivatives. Comput and Struct 1998; 69:247–54.
[17] Ting TCT, Lee V-G. The three-dimensional elastostatic Green's function for general anisotropic linear elastic solids. Q J Mech Appl Math 1997;50(3):407–26.
[18] Ting TCT. Recent developments in anisotropic elasticity. Int J Solids Struct 2000;37:401–9.
[19] Deans SR. The Radon transform and some of its applications. New York: Wiley Interscience, 1983.
[20] John F. Plane waves and spherical means applied to partial differential equations. New York: Interscience; 1955.
[21] Gel'fand IM, Graev MI, Vilenkin, YN. Generalized functions, vol. 5. New York: Academic Press; 1966.
[22] Helgason S. The Radon transform birkhauser. Basel: Boston; 1980.
[23] Courant R, Hilbert D. Methods of mathematical physics, vol. II. New York: Interscience; 1962.